Lasers in Manufacturing Conference 2015

Influence of Ambient Pressure on Spatter Formation during Laser Welding of Copper

Andreas Heider[a]*, Thomas Engelhardt[b], Rudolf Weber[a], Thomas Graf[a]

[a]*Institut für Strahlwerkzeuge (IFSW), University of Stuttgart, Pfaffenwaldring 43, 70569 Stuttgart, Germany*
[b]*Daimler AG, Mercedesstr. 137, 70327 Stuttgart, Germany*

Abstract

Due to its high electrical and thermal conductivity, copper has a wide range of applications. Many of those require an efficient and reliable welding process most preferably using a remote laser technique. However, the low absorptivity of copper at the wavelength of 1 µm together with its high heat conductivity makes remote laser welding of copper a challenging task. Welding speeds below 10 m/min are required to obtain penetration depths of several millimeters in copper when using laser sources with average powers below about 8 kW. Such welds suffer from numerous defects such as melt ejections and pores. As these weld defects degrade both, the mechanical and electrical properties of the weld seam, it is important to reduce or even avoid such weld defects especially for industrial applications.

For the present paper the influence of the ambient pressure on defect formation was investigated. High-speed X-ray imaging of the welding process was used to analyze keyhole stability. It was seen that spatter formation was strongly reduced for reduced ambient pressure. Simultaneously, the penetration depth was decreased of up to 40% using identical laser parameters. It was seen that changing the ambient pressure directly correlates with a change of both, the shape and the stability of the keyhole.

Keywords: Welding Copper; Laser welding; X-ray; Reduced pressure; Vacuum; Process stabilization; Spatters; Pores; Ejections.

1. Introduction

Pure copper (e.g. Cu-ETP) and many copper alloys are more and more in demand for industrial applications due to their high electrical and thermal conductivity. However, the optical and thermal material

* Andreas Heider. Tel.: +49-(0)711-685-69730; fax: +49-(0)711-685-59730.
E-mail address: andreas.heider@ifsw.uni-stuttgart.de.

properties make laser welding of copper a very challenging task. Due to the low absorptivity of only a few percent at a wavelength of 1 µm and due to the high heat conductivity, comparatively low welding speeds of less than 10 m/min are needed to achieve welds with penetration depths of ≥ 1 mm using commercially available lasers with a few kW of laser power [Heß 2012 and Petring 2010]. Laser remote welding of copper at welding speeds of less than 10 m/min frequently shows numerous weld defects such as pores and holes in the weld seam [Blom, 2003 and Engler, 2011 and Heß, 2010 and Heider 2011].

Fig. 1 (a1-a4) shows the typical formation of a melt ejection in a series of single frames out of a high-speed video of a welding process in pure copper (Cu-ETP). Starting from the regular process (a1) first the volume of the melt pool expands (a2) before the molten material is explosively blown out of the interaction zone (a3). As this leaves a hole surrounded by solid material (a4) the keyhole and the melt pool subsequently has to be reformed as at the beginning of a welding process. As such instabilities occur quite frequently the weld seams are characterized by numerous ejections and pores [Heider, 2011] as seen from the top view in Fig. 1 (b) and the longitudinal cross section (c) of a weld in Cu-ETP. The bottom picture (c) illustrates that the holes which are formed by the melt ejections are mostly as deep as the weld seam depth which is marked by the dashed white line. As these weld defects degrade both, the mechanical and the electrical properties of the weld seam it is important to avoid or at least minimize the number of such defects.

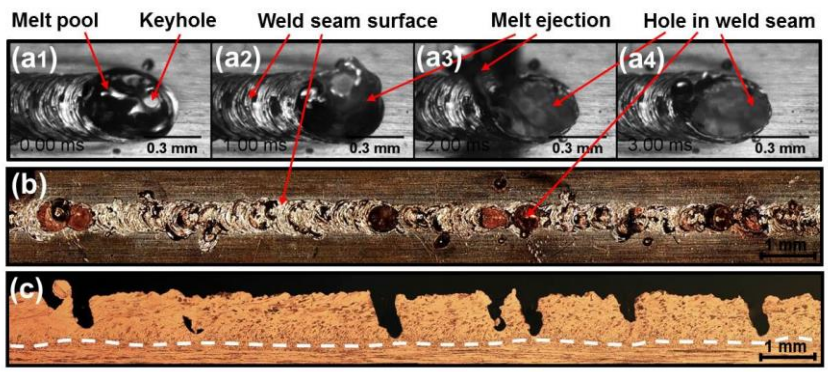

Fig. 1: Series of single frames out of a high-speed video of a welding process in Cu-ETP showing the formation of a melt ejection (a1-a4). Top-view (b) and longitudinal cross-section (c) of a weld seam in Cu-ETP; welded with a welding speed of 6 m/min and an incident laser power of 1500 W at a wavelength of 1 µm. The white dashed line indicates the penetration depth of the welding seam.

Keyhole instabilities are described to be one of the reasons for weld defects [Fabbro, 2006]. To experimentally analyze the process dynamics such as keyhole and melt pool dynamics usually high-speed observation in the visible wavelength range is applied. With this technique only the sample surface can be observed whereas no information of the behavior inside the material can be obtained. By means of high-speed X-ray diagnostics during welding, phenomena such as the keyhole dynamics or spatter formation and pore formation can be analyzed [Matsunawa, 1998]. Using X-ray technique it was shown that welding of aluminum and steel at reduced pressure no pore formation and less spattering occurred. In addition previous studies of laser welding of steel and aluminum have shown a strong increase of the welding depth with decreasing pressure [Verwaerde, 1995 and Katayama, 2001 and Katayama, 2011].

1.1. Formation of a melt ejection

Keyhole instabilities during welding are known to be one cause for the observed weld defects [Fabbro, 2006 and Kaplan, 2002]. Keyhole instabilities can occur when the power density in the keyhole is too low to maintain the evaporation pressure to keep the keyhole open [Tsukamoto, 2003]. With high-speed X-ray observation it was shown that bubble formation at the tip of the keyhole is directly correlated to the formation of melt ejection at welding copper [Heider, 2013]. In Fig. 2 single frames out of a high-speed X-ray video of a copper weld are shown. The sequence shows the formation of a melt ejection.

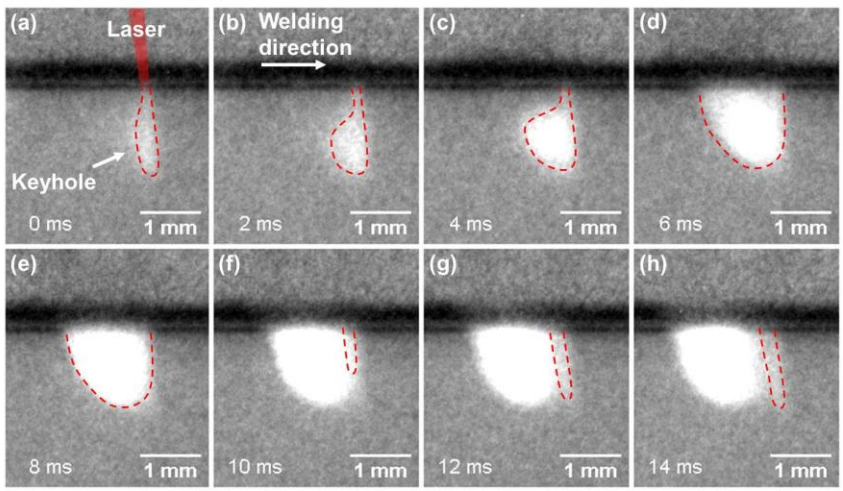

Fig. 2: Single frames out of a high-speed X-ray video of a weld in Cu-ETP. Bubble formation at welding copper. P = 3 kW, v = 4 m/min, d_f = 100 µm.

A narrow and straight capillary can be observed at the initial X-ray image (Fig. 2 (a), lighter grey area outlined with the red dashed line). After 2 ms the backside in the lower part of the keyhole begins to expand and a bubble like structure at the tip of the keyhole appears (b). Within the next 4.0 ms growing of the bubble occurs (b – d). The bubble size increases dramatically within less than 2 ms (c-d) leading to an almost complete ejection of the whole molten material out of the interaction zone (e). Subsequently the keyhole has to be reformed (f-h).

The bubble pushes the molten material in direction of the sample surface leading to a swelling of the weld seam surface (c-d). Growing of the bubble continues as long as the surface tension is larger than the pressure created by the bubble. From this sequence it can be concluded that if a critical bubble size is exceeded a melt ejection is generated. Therefore the formation of bubbles at the tip of the capillary is one of the reasons for the development of melt ejections. Means to avoid bubble formation at the tip of the capillary and a more detailed description of the formation of melt ejections are e.g. presented in Heider, 2011 and Heider, 2013 and Heider, 2015.

In this paper the results of X-ray observation of the keyhole behavior in copper welding at reduced ambient pressures are shown. The stability of the keyhole and the formation of melt ejections and pores are discussed.

2. Experimental Set-Up

A cw thin-disk Yb:YAG laser (TruDisk 5001) with a wavelength of 1030 nm and a maximum output power of 5000 W was used for the investigations. The beam was delivered through a fiber with a numerical aperture of 0.1 and a core diameter of 100 µm. The beam was collimated with a lens with a focal length of 200 mm and focused with a lens with a focal length of 300 mm. The focus diameter on the work piece was 150 µm. All welds were observed and recorded with a high-speed camera at frame rates of 10 kHz. The sample surface was illuminated by a diode laser with a wavelength of 808 nm and the camera was equipped with the corresponding band pass filter. The welded samples were 2.5 mm wide, 20 mm in height and 100 mm long (in the direction of the seam) for all experiments. All welds were 40 mm long performed with partial penetration and without shielding gas.

High-speed online X-ray technique was used to observe the keyhole behavior and phenomena inside the sample while welding. The X-ray imaging system consists of a micro-focus X-ray tube generating the X-ray radiation and an imaging system converting the X-ray radiation to visible light. The X-ray imaging setup is shown in Fig. 3 (a).

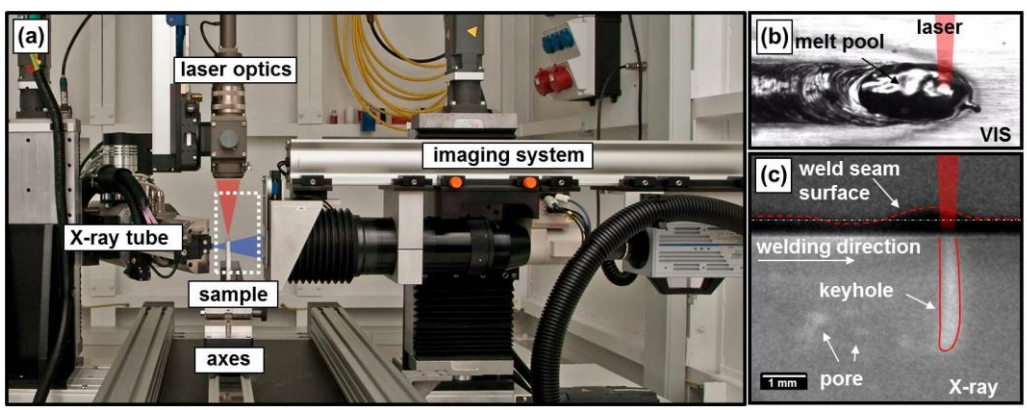

Fig. 3: (a) High-speed imaging X-ray system. (b) Single frame out of a high-speed observation of sample surface. (c) Single frame out of a high-speed X-ray observation of a weld [Abt, 2011].

Fig. 3 (a) shows the set-up without vacuum chamber. The micro focus of the electron beam in the X-ray tube has a minimum spot size 6 µm. Typical operation spot sizes however are in the range from 50 µm to 150 µm The sample is X-rayed in horizontal direction. For welding, the laser beam irradiates the sample from the top and impacts the material at the narrow side of the sample. The white dashed line illustrates the position where the vacuum chamber was mounted. In Fig. 3 (b) a single image of a high-speed video of the sample surface and the corresponding single frame of the X-ray observation of the weld is shown (Fig. 3 (c)). The relevant features are outlined [Abt, 2011]. The laser beam (marked with the red area) hits the sample surface and creates a deep and narrow capillary. Due to the lower density of vaporized material inside the keyhole, the keyhole is visible as a lighter grey area outlined with the continuous red line. In addition to the keyhole, pores can be seen on the left hand side of the keyhole tip as lighter grey circle areas. The dashed red line above the black area shows the weld seam surface. The welding direction is from the left to the right.

All experiments were performed with an additional vacuum chamber mounted between the X-ray tube and the imaging system. A schematic sketch of the vacuum chamber from two sides and the relevant features are shown in Fig. 4. The laser beam irradiates the sample from the top. The sample was clamped on a wagon of iron. A magnet fixed on the moving axes outside of the vacuum chamber was used for the movement of the

wagon and the sample inside the chamber through magnetic forces. A vacuum pump was used to evacuate the chamber. An adjustable gas flow of nitrogen was used to set the pressure inside the chamber. The pressure was monitored with a pressure monitor. A slight N_2-gas flow was used to prevent contamination of the protective window due the metal vapor or spattering. For observation with high-speed cameras an additional window was used.

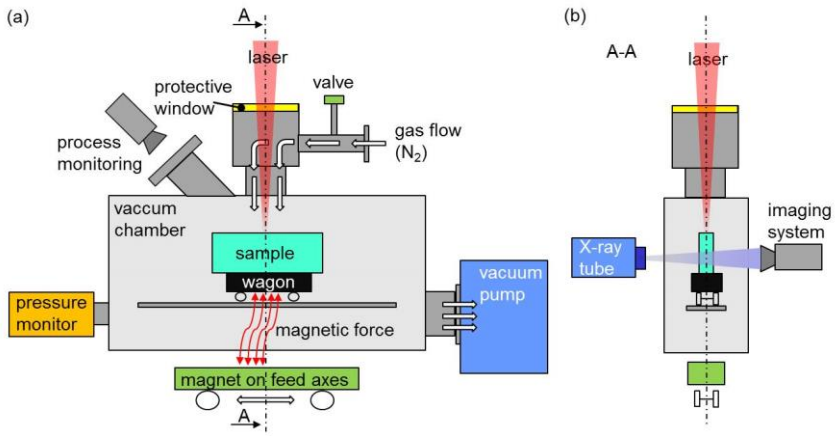

Fig. 4: Schematic sketch of the vacuum chamber.

Samples of pure copper (Cu-ETP) were used for the experiments. The relevant thermo-physical properties are summarized in Table 1.

Table 1: Material properties of the copper materials under investigation at ambient temperature and atmospheric pressure [Wieland Werke 2011].

Properties	E-Cu-58 (Cu-ETP)
Heat conductivity k [W/(mK)]	390
Heat capacity c_p [J/(gK)]	0.386
Density r [g/cm³]	8.93
Thermal diffusivity κ=k/(rc$_p$) [cm²/s]	1.131

For the determination of the welding depth all samples were cut, polished and etched allowing an accuracy of the measured welding depth of less than ± 100 µm. The penetration depth for the samples welded with constant laser power was measured from cross sections. The penetration depth for the samples welded with a power ramp was measured from longitudinal cross sections every fifth millimeter at eight positions along the weld. In addition the keyhole depth was measured form X-ray videos as an indicator for the penetration depth.

3. Results

Welds using the setup shown in Fig. 4 were performed at atmospheric pressures of about 1000 mbar (reference pressure), 500 mbar, 50 mbar and 5 mbar. In the following the atmospheric pressure is referred to as “1000 mbar”. Welds at different constant laser powers of 3 kW and 5 kW at welding speeds of 4 m/min and 6 m/min were made. In addition power ramps from 3 kW to 5 kW of laser power at 4 m/min welding

speed were performed. The focal position was measured several times at each pressure. No change in focal position was measured. Therefore an influence of thermal effects or deformation of optical elements could be excluded. Fig. 5 shows the penetration depth as a function of the laser power for different ambient pressures at a welding speed of 4 m/min. The laser power was increased continuously from 3 kW to 5 kW. For every pressure the penetration depth increases with increasing laser power. The increase in penetration depth is much more significant for the weld at 1000 mbar compared to the weld at 5 mbar. At a laser power of 4750 W the penetration depth at 1000 mbar is about 40% higher compared to the penetration depth at 5 mbar.

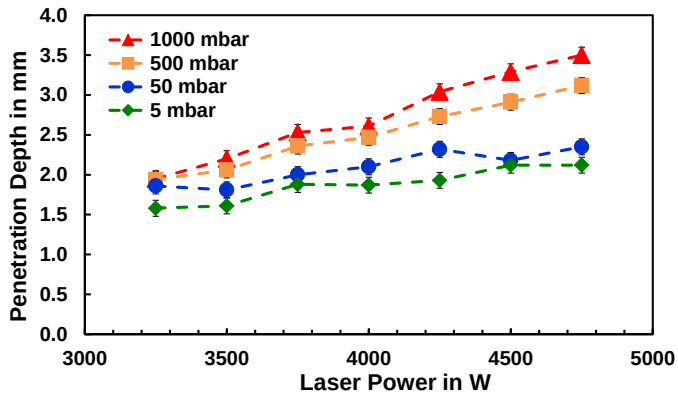

Fig. 5: Penetration depth as a function of the laser power for welds in Cu-ETP at different ambient pressures. P = 3 kW – 5 kW, v = 4 m/min, d_f = 150 µm.

In Fig. 6 images of the weld seam surface (b1, c1) and the corresponding longitudinal cross sections (b2, c2) to the results of Fig. 5 are depicted. The dashed black lines in the longitudinal cross sections illustrate the penetration depth. Fig. 6 (a) shows a sketch of the used power ramp from 3 kW to 5 kW.

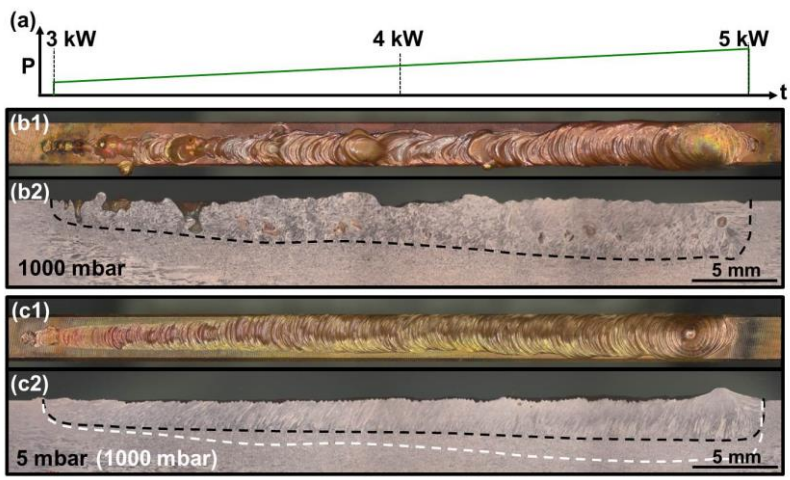

Fig. 6: Images of the weld seam surface (b1, c1) and the corresponding longitudinal cross sections (b2, c2) of welds in Cu-ETP at different ambient pressure. (b) 1000 mbar, (c) 5 mbar. Dashed lines show the penetration depth. P = 3 – 5 kW, v = 4 m/min, d_f = 150 µm. (a) sketch of the used power ramp.

The image (b) shows the reference weld at 1000 mbar. The weld seam surface and the longitudinal cross section at 5 mbar are shown in Fig. 6 (c). For comparison, the penetration depth of the weld at 1000 mbar is added to the image of the weld at 5 mbar (white dashed line). Comparing the welds numerous holes in the weld seam due to melt ejections and pores can be seen especially for the lower power region (3 kW to 4 kW) for the 1000 mbar weld. Whereas a very homogeneous weld seam surface without any melt ejections are observed for the 5 mbar weld. The results of Fig. 6 clearly show that with reducing ambient pressure at welding copper weld defects such as melt ejection and spatter formation can strongly be reduced.

4. Discussion

As mentioned above keyhole instabilities during welding are known to be one cause for the observed weld defects [Fabbro, 2006 and Kaplan, 2002]. Therefore the keyhole shape was investigated for the different ambient pressures. In Fig. 7 single frames out of high-speed video observation from the sample surface (a1-d1) and the corresponding frames out of X-ray observation of the keyhole shape (a2-d2) 17 ms (1.7 mm) after process start are compared for different pressures. The laser power was kept constant at 5 kW at a welding speed of 6 m/min. 17 ms after process start the keyhole diameter at the sample surface (see Fig. 7 (a1 – d1)) as well as the shape and keyhole depth (see Fig. 7 (a2 – d2)) have nearly the same dimensions for all investigated pressures.

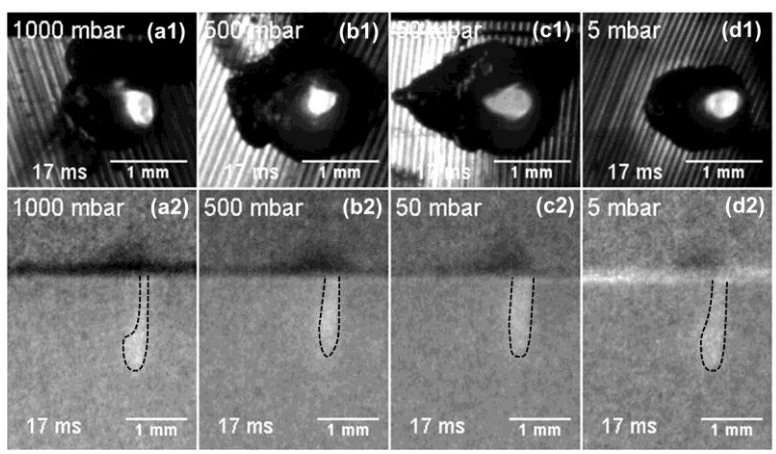

Fig. 7: Single frames out of a high-speed video from the sample surface (1) and corresponding single frames out of an X-ray video (2) at different ambient pressure (a-d), 17 ms after process start. P = 5 kW, v = 6 m/min, d_f = 150 µm.

Fig. 8 shows the same weld as Fig. 7 at 233 ms after the process start. Again single frames out of high-speed video observation from the sample surface (a1-d1) and the corresponding frames out of X-ray observation of the keyhole shape (a2-d2) 233 ms after process start are compared. At the pressure of 1000 mbar a circular keyhole shape at the sample surface (Fig. 8 (a1)) is observed.

The characteristic keyhole shape with a bubble like structure at the tip of the keyhole can be seen. With decreasing ambient pressure (b-d) the keyhole area at the sample surface enlarges. Furthermore keyhole shape below the sample surface strongly changes. The complete keyhole expands against the direction of welding and no significant bubble formation at the tip of the keyhole is visible. In addition the keyhole depth decreases with decreasing pressure which is in good agreement with the results shown in Fig. 5. Up to now there is no explanation for the transition from the deep keyhole at the process start (see Fig. 7) to the increased keyhole

diameter and the decrease in keyhole depth at 5 mbar (see Fig. 8). One cause for the lower penetration depth at lower pressure might be the increased keyhole diameter.

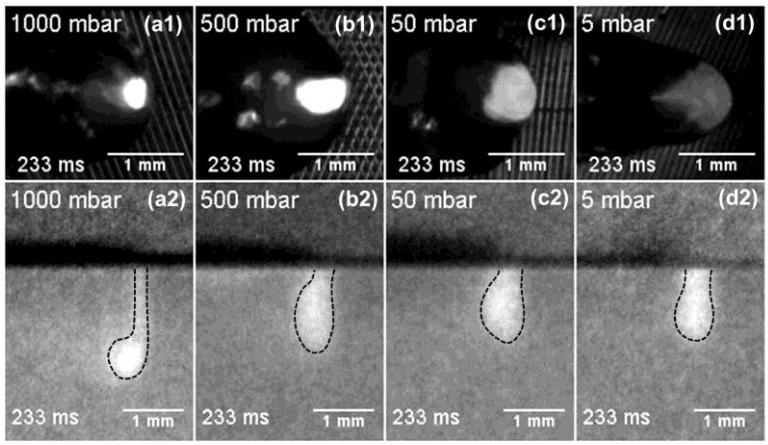

Fig. 8: Single frames out of a high-speed video from sample surface (1) and corresponding single frames out of an X-ray video (2) at different ambient pressure (a-d), 233 ms after process start. P = 5 kW, v = 6 m/min, d_f = 150 µm.

Fig. 9 shows single frames of an X-ray video from a weld at 5 mbar from 15 ms to 90 ms after the process start at the constant power of 5 kW. After 15 ms (a) a deep and narrow keyhole is formed. After 40 ms (b) the keyhole enlarges and the keyhole depth decreases until a constant keyhole shape is reached (c-d). No bubble formation at the tip of the keyhole occurs.

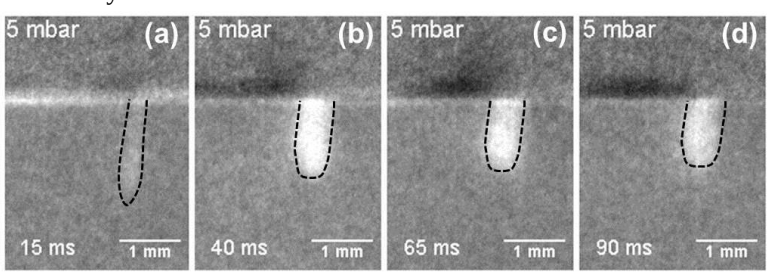

Fig. 9: Single frames out of an X-ray video from a weld at 5 mbar. P = 5 kW, v = 6 m/min, d_f = 150 µm.

The described behavior is in good agreement to the results of Fig. 6. At the beginning of the weld only a slight deviation in penetration depth of the weld in Fig. 6 for the weld at 5 mbar compared to 1000 mbar can be seen. The deviation in penetration depth increases after about 40 ms for the weld at 5 mbar compared to 1000 mbar.

5. Conclusion

Welds in pure copper were made with a variation of the ambient pressure. It was seen that spatter formation was strongly reduced for reduced ambient pressure. Simultaneously, the penetration depth was decreased of up to 40% using identical laser parameters. It was seen that changing the ambient pressure directly correlates with a change of both, the shape and the stability of the keyhole. The keyhole enlarges with reduced pressure and bubble formation at the tip of the keyhole could be suppressed.

References

Heß, A. 2012. Vorteile und Herausforderungen beim Laserstrahlschweißen mit Strahlquellen höchster Fokussierbarkeit. Ph.D. Thesis University of Stuttgart (IFSW) Germany.

Petring, D. and Goneghany, V. N. 2010. Learning more about laser beam welding by applying it to copper and copper alleys. Proc. of 29th International Congress on Applications of Lasers and Electro-Optics ICALEO (USA, Anaheim, CA).

Blom, A. et al. and de Kramer, J. 2003. Process spread reduction of laser micro-spot welding of thin copper parts using real-time control. Proc. of SPIE Vol. **4977.**

Engler, S., Ramsayer, R. and Poprawe, R. 2011. Process Studies on Laser Welding of Copper with Brilliant Green and Infrared Lasers. In Physics Procedia **12**, 342 - 349.

Heß, A. et al. 2010. Forced deep-penetration welding with low-power second-harmonic assistance of cw copper welding with 1 µm wavelength. Proc. of 6th International Congress Laser Assisted Net Shape Engineering LANE (Germany, Erlangen).

Heider, A. et al. 2011. Process Stabilization at welding Copper by Laser Power Modulation. In Physics Procedia **12**, 81-87.

Fabbro, R. et al. 2006. Experimental study of dynamical coupling between the induced vapour plume and the melt pool for Nd-Yag CW laser welding. J. Phys. D; Appl. Phys. Vol. **39**.

Matsunawa, A. at el. 1998. Dynamics of keyhole and molten pool in laser welding J. Laser Appl. Vol. **10** 247–54.

Verwaerde, A., Fabbro, R. and Deshors, G. 1995. Experimental study of continuous CO2 laser welding at subatmospheric pressures J. of Appl. Phys. **78** (5), Vol. **2981.**

Katayama, S. et al. 2001. Effect of vacuum on penetration and defects in laser welding J. of Laser Appl. Vol. **13**, Nr. **5**.

Katayama, S. et al. 2011. Development of Deep Penetration Welding Technology with High Brightness Laser under Vacuum, in Physics Procedia 12, 75-80.

Abt, F. et al. 2011. X-Ray videography for investigation of capillary and melt pool dynamics in different materials“, Proceedings in ICALEO, Orlando, USA.

Wieland Werke 2011 Copper data sheet of B16 (CuSn6) and K32 (E-Cu-58) www.wielandwerke.de.

Matsunawa, A. et al. 1998 Dynamics of keyhole and molten pool in laser welding“, J. of Laser Applications, Volume **10**, Nr. 6.

Tsukamoto, T. et al. 2003. Keyhole Behaviour in High Power Laser Welding Proc. of SPIE Vol. 4831.

Kaplan, A. et al. 2002. Unbounded keyhole collapse and bubble formation during pulsed laser interaction with liquid zinc J. Phys. D: Appl. Phys. **35**, 1218–1228.

Heider, A. et al. 2013. Investigation of Spatter Formation in Laser Welding of Copper using High-Speed Online X-Ray Imaging Proc. of LAMP2013 the 6th International Congress on Laser Advanced Materials Processing (Niigata, Japan).

Heider, A. et al. 2015. Power modulation to stabilize laser welding of copper. J. Laser Appl. Vol. **27**, Nr. 2, p. 022003. DOI: 10.2351/1.4906127